bioRxiv preprint doi: https://doi.org/10.1101/613315; this version posted April 1, 2020. The copyright holder for this preprint (which was not certified by peer review) is the author/funder, who has granted bioRxiv a license to display the preprint in perpetuity. It is made available under aCC-BY-NC 4.0 International license.

Iron is a ligand of SecA-like metal-binding domains *in vivo*

Tamar Cranford-Smith[a,1], Mohammed Jamshad[a,1], Mark Jeeves[b], Rachael A. Chandler[a], Jack Yule[a], Ashley Robinson[a], Farhana Alam[a], Karl A. Dunne[a], Edwin H. Aponte Angarita[a,c], Mashael Alanazi[a,d], Cailean Carter[a], Ian R. Henderson[a,†], Janet E. Lovett[e], Peter Winn[a,c], Timothy Knowles[a] and Damon Huber[a,*]

[a]Institute for Microbiology and Infection, [b]Institute of Cancer and Genomic Sciences and [c]Centre for Computational Biology, University of Birmingham, Birmingham, United Kingdom; [d]Department of Biology, College of Science, Jouf University, Saudi Arabia; [e]SUPA, School of Physics and Astronomy and BSRC, University of St Andrews, St. Andrews, United Kingdom

Running title: *SecA-like MBDs bind to iron*

[1]These authors contributed equally to this work.

*Address correspondence to: Damon Huber, d.huber@bham.ac.uk

[†]Present address: Institute for Molecular Bioscience, University of Queensland, St. Lucia, Brisbane, Australia

Keywords: SecA, Sec, protein translocation, protein transport, metal binding, iron, zinc, NMR, EPR

ABSTRACT

The ATPase SecA is an essential component of the bacterial Sec machinery, which transports proteins across the cytoplasmic membrane. Most SecA proteins contain a long C-terminal tail (CTT). In *Escherichia coli*, the CTT contains a structurally flexible linker domain and a small metal-binding domain (MBD). The MBD coordinates zinc via a conserved cysteine-containing motif and binds to SecB and ribosomes. In this study, we screened a high-density transposon library for mutants that affect the susceptibility of *E. coli* to sodium azide, which inhibits SecA-mediated translocation. Results from sequencing this library suggested that mutations removing the CTT make *E. coli* less susceptible to sodium azide at subinhibitory concentrations. Copurification experiments suggested that the MBD binds to iron and that azide disrupts iron binding. Azide also disrupted binding of SecA to membranes. Two other *E. coli* proteins that contain SecA-like MBDs, YecA and YchJ, also copurified with iron, and NMR spectroscopy experiments indicated that YecA binds iron via its MBD. Competition experiments and equilibrium binding measurements indicated that the SecA MBD binds preferentially to iron and that a conserved serine is required for this specificity. Finally, structural modelling suggested a plausible model for the octahedral coordination of iron. Taken together, our results suggest that SecA-like MBDs likely bind to iron *in vivo*.

INTRODUCTION

Translocation of proteins across the cytoplasmic membrane is carried out by the evolutionarily conserved Sec machinery (1,2). The central component of this machinery is a channel in the cytoplasmic membrane, which is composed of the proteins SecY, -E and -G in bacteria (3). The translocation of a subset of proteins through SecYEG requires the activity of the ATPase SecA (4,5). In *Escherichia coli*, SecA contains 901 amino acids. The N-terminal ~830 amino acids of SecA in *E. coli* make up the catalytic core of the protein, which is essential for viability and is sufficient to reconstitute protein translocation *in vitro* (6-9). The C-terminal ~70 amino acids (C-terminal tail; CTT) are widely, but not universally, conserved (10). The CTT contains two regions: a structurally flexible linker domain (FLD) and a small metal-binding domain (MBD). The amino acid sequence of the FLD is poorly conserved, and recent research suggests that the FLD autoinhibits the activity of SecA by stabilising a conformation of SecA with a lower affinity for substrate protein (10,11). When

bioRxiv preprint doi: https://doi.org/10.1101/613315; this version posted April 1, 2020. The copyright holder for this preprint (which was not certified by peer review) is the author/funder, who has granted bioRxiv a license to display the preprint in perpetuity. It is made available under aCC-BY-NC 4.0 International license.

present in SecA, the sequence of the MBD is highly conserved (10). The MBD interacts with SecB and ribosomes (10,12), and interaction of the MBD with SecB or ribosomes relieves MBD-mediated autoinhibition (10,11). The MBD binds to a single Zn^{2+} ion (12), which is coordinated by three conserved cysteines and a histidine with a conserved $CXCX_8CH$ ($CXCX_8CC$ in some bacteria) motif (**supporting figure S1**) (10,12,13). In addition, the MBD contains several highly conserved amino acids, including Ser-889 and Tyr-893, whose functional significance is unknown (10,13,14).

Sodium azide is a well studied inhibitor of SecA (15-18). Azide causes a nearly complete block in SecA-mediated protein translocation within minutes of addition to growing cells (15), and mutations that confer increased resistance to azide map to the *secA* gene (15-17). Azide is thought to inhibit nucleotide exchange by SecA (19,20). Indeed, most of the mutations that confer azide resistance modify amino acids in one of the two nucleotide binding domains (17), and many of these substitutions increase the rate of nucleotide exchange in *in vitro* assays (20). However, the concentration of azide required to partially inhibit the rate of ATP turnover by SecA *in vitro* (10-20 mM) is much higher than that required block translocation *in vivo* (1-2 mM) (15,21), suggesting that azide-mediated inhibition of SecA *in vivo* is more complex.

In order to gain insight into the effect of azide on protein translocation *in vivo*, we determined the effect of azide on the relative growth rates of >1 million independent transposon mutants using transposon-directed insertion-site sequencing (TraDIS) (22,23). The results of this screen suggested that azide caused CTT-mediated autoinhibition of SecA, potentially by disrupting the MBD. Treating cells with azide reduced the amount of iron (but not zinc) that co-purified with the MBD to background levels, suggesting that a subpopulation of SecA proteins bind to iron and that azide triggers autoinhibition by disrupting the MBDs of this subpopulation. Full-length SecA produced at more physiological levels copurified predominantly with iron. Furthermore, two *E. coli* proteins containing SecA-like MBDs, YecA and YchJ, bind to and copurify with iron. Biophysical characterisation of metal binding properties of YecA and SecA indicated that their MBDs bind to iron, and competition experiments and equilibrium binding measurements suggest that the MBD of SecA binds preferentially to iron. Finally, our results suggest that an evolutionarily conserved serine residue is important for mediating this specificity. Taken together, our results indicate that iron is a physiological ligand of SecA-like MBDs.

RESULTS

Identification of genes that affect the susceptibility of E. coli to sodium azide. To gain insight into the effect of azide on cells, we identified transposon mutations that influence the susceptibility of *E. coli* to azide using TraDIS (22,23). To this end, we determined the concentration of azide that inhibited, but did not prevent, the growth of *E. coli* BW25113. Growth curves in the presence of increasing concentrations of azide indicated that 250 and 500 μM sodium azide were the highest concentrations that did not completely inhibit growth in LB (**supporting figure S2**). We then grew a library of > 1 million independent BW25113 mini-Tn*5* transposon mutants (23) in the presence of subinhibitory concentrations of azide and determined the change in the relative proportion of mutations in each insertion using Illumina sequencing. Growth of the library in the presence of 0.25 mM or 0.5 mM azide resulted in a strong depletion (> $\log_2$ 1.5-fold) in insertions in approximately 180 of the 4346 genes included in the analysis. Many of the most strongly depleted insertions disrupted genes encoding components of the Sec machinery (e.g. *yajC*, *secG*, *secF*, *secM*, *yidC*) or cell envelope stress responses (e.g. *cpxR*, *dsbA*) (**figure 1A; supporting data S1**), consistent with the ability of azide to inhibit Sec-dependent protein translocation and disrupt biogenesis of the cell envelope.

To verify the results of the TraDIS screen, we investigated the effect of subinhibitory azide on individual mutants. Mutants containing insertions in the *secG*, *yajC*, *dsbA*, *cpxR*, *gor*, *ahpC* and *trxC* genes were strongly to moderately depleted during growth in the presence of azide. With the exception of the Δ*gor* mutant, cells containing deletion mutations in these genes grew more slowly than the parent in the presence of azide (**table 1**).

The presence of azide also caused a strong enrichment in mutants containing insertions in the *secA* gene at codon 822 (**figure 1B**), consistent with the requirement for the N-terminal portion of SecA

bioRxiv preprint doi: https://doi.org/10.1101/613315; this version posted April 1, 2020. The copyright holder for this preprint (which was not certified by peer review) is the author/funder, who has granted bioRxiv a license to display the preprint in perpetuity. It is made available under aCC-BY-NC 4.0 International license.

for viability. Growth in the presence of azide resulted in a strong enrichment in insertions truncating SecA between amino acids 822 and 829, resulting in a complete truncation of the CTT (**figure 1B**). In addition, a strain containing a mutation that truncates SecA at amino acid ~827 (*secA827*::IS*3*) (6) grew more rapidly than the parent strain in exponential phase in the presence of sodium azide (**table 1**). Despite the increased growth rate at subinhibitory concentrations of azide, this mutant did not detectably influence the MIC of azide in filter disc assay (data not shown). These results suggested that azide causes autoinhibition of SecA at concentrations that are subinhibitory for growth.

Effect of azide on binding of SecA to membrane phospholipids. We next investigated the effect of azide on binding of SecA to membranes. Previous studies indicate that SecA binds strongly to membranes (24-28), and a protein fusion between hexa-histidine-tagged SUMO and SecA (His-SUMO-SecA) copurified strongly with membrane phospholipids (**figure 1C**). Expression of this fusion protein can complement the conditional growth defect of a strain producing SecA under control of an arabinose-inducible promoter, indicating that it is functional *in vivo*. Previous studies have suggested that the CTT is involved in binding phospholipids (29). Indeed, His-SUMO-SecA containing alanine substitutions in two of the metal-coordinating cysteines (C885 and C887; His-SUMO-SecA$^{CC/AA}$) did not copurify with phospholipids (**figure 1C**). His-SUMO-SecA purified from cells treated with azide prior to lysis did not copurify with phospholipids, indicating that azide disrupts binding of SecA to the membrane (**figure 1C**). Furthermore, washing purified His-SUMO-SecA disrupted binding to phospholipids *in vitro* (**supporting figure S3**). These results suggested that azide could disrupt the structure of the MBD.

Effect of azide on the MBD of SecA. To investigate the ability of azide to disrupt the structure of the MBD, we determined the metal content of a fusion protein between SUMO and the CTT (SUMO-CTT). ICP-MS indicated that SUMO-CTT copurified with significant amounts of zinc, iron and copper. Treating cells with azide prior to lysis did not affect the amount of zinc or copper that copurified with SUMO-CTT. However, there was a strong reduction in the amount of iron that copurified with SUMO-CTT from azide treated cells (**figure 2A**), raising the possibility that iron is the physiological ligand of the MBD. In addition, SUMO-CTT purified from azide-treated cells was more prone to aggregation than SUMO-CTT purified from untreated cells (**supporting figure S4**), consistent with the notion that azide treatment disrupts the structure of the MBD. Finally, the presence of the metal-chelator EDTA in the growth medium increased the sensitivity of *E. coli* to azide, while the addition of excess $FeSO_4$, but not $ZnSO_4$, to the growth media decreased sensitivity to azide (**supporting table S1**), supporting the idea that azide disrupts the iron-bound form of SecA.

Co-purification of SecA-biotin with iron. Purification of SecA normally involves overproduction of the protein, followed by multiple purification steps, which could lead to mis-metallation or metal exchange. To determine whether full-length SecA binds to metal *in vivo*, we produced SecA from a chromosomally encoded, IPTG-inducible copy of the *secA* gene. The SecA produced by these strains contained a C-terminal tag that caused it to be biotinylated (SecA-biotin) (30) and allowed us to purify it using streptavidin-coated sepharose beads. SDS-PAGE indicated that the purified protein samples contained only two proteins: SecA and unconjugated streptavidin (**supporting figure S5**). ICP-OES indicated that iron was present at much higher concentrations in the protein samples than zinc (**figure 2B**), suggesting that SecA binds to iron *in vivo*.

EPR analysis of Fe^{3+} binding by the SecA MBD. Previous work indirectly suggested that the MBD has a lower affinity for iron than for zinc (12). To demonstrate that the MBD of SecA can bind to iron, we investigated the effect of the MBD on the EPR spectrum of Fe^{3+}. (Fe^{2+} is not detectable by EPR.) The addition of a metal-free synthetic peptide consisting of the C-terminal 27 amino acids of SecA (SecA-MBD) caused a large increase in the EPR signal of Fe^{3+} at 1.2155 T (~g = 2) and altered the shape of the EPR spectrum (**figure 2C**). SecA-MBD also inhibited the formation of insoluble precipitates (possibly iron oxides) in solutions containing $FeSO_4$ (**supporting figure S6**). These results indicated that SecA-MBD can bind iron.

Mass spectrometry analysis of metals that co-purify with YecA and YchJ. Fourteen open reading frames in *E. coli* encode polypeptides with the amino acid sequence $CXCX_NCH$ or

bioRxiv preprint doi: https://doi.org/10.1101/613315; this version posted April 1, 2020. The copyright holder for this preprint (which was not certified by peer review) is the author/funder, who has granted bioRxiv a license to display the preprint in perpetuity. It is made available under aCC-BY-NC 4.0 International license.

$CXCX_NCC$: SecA, YecA, YchJ, YjbI, QuuD, ribosomal protein L31, ferredoxin, HCR, YgeH, GlcF, NirB, YjiM, HypA and YeaX (**supporting data S2**). According to UniProt (31), all eight of the proteins with well characterised functions (SecA, L31, ferredoxin, HCR, GlcF, NirB, HypA and YeaX) bind to a metal using all or part of this sequence, and five (ferredoxin, HCR, GlcF, NirB and YeaX) are annotated as binding to iron. Of the remaining proteins, YecA and YchJ contain C-terminal domains, each of which has 73% sequence identity to amino acids 878-899 of SecA. (The C-terminal 22 amino acids of YecA and YchJ are 77% identical to each other.) In addition to the metal-coordinating cysteines, these sequences contain the conserved serine and aromatic residues (**supporting figure S1**). The N-terminal portion of YchJ contains a second $CXCX_NCC$ motif, which also contains the conserved serine and aromatic residues found in the SecA MBD.

The finding that the SecA MBD binds to iron suggested that YecA and YchJ could also bind to iron. To investigate the metal-binding properties of YecA and YchJ, we purified fusion proteins between YecA or YchJ and hexahistidine-tagged SUMO from *Saccharomyces cerevisiae* and determined the amount of copurifying manganese, iron, cobalt, copper and zinc by ICP-MS. YecA co-purified with zinc at a stoichiometry of 0.84 ± 0.03, consistent with the presence of a single MBD (**figure 3A**). YchJ co-purified with zinc at a stoichiometry of 1.30 ± 0.17 (**figure 3A**), consistent with the presence of two MBDs. Both proteins also copurified with lower, but detectable, amounts of copper (0.17 ± 0.11 for YecA; 0.02 ± 0.01 for YchJ) and iron (0.04 ± 0.03 for YecA; 0.05 ± 0.04 for YchJ).

Absorbance spectroscopy of purified YecA and YchJ. During purification, the colour of the YecA- and YchJ-bound Ni-NTA columns was yellow. If TCEP was included in the buffers used for purification of YecA, the Ni-NTA column remained yellow after elution of the bound protein. Ni-NTA columns are blue-green due to the coordinated Ni^{2+} ion and normally regain this colour after elution of the bound protein with imidazole. The change in colour suggested that the bound Ni^{2+} had exchanged with another metal ion, presumably from the overexpressed protein in the cell lysate used for purification. Analysis of the EDTA eluate indicated that the bound metal ion was iron (**supporting figure S7**). Furthermore, purified YecA and YchJ were pale yellow in colour (Zn-bound proteins are normally colourless) and gradually became colourless with incubation at 4°C—typically over a period of one to several hours. YecA absorbed light with a peak at ~330 nm, and YchJ absorbed light with a peak at ~340 nm (**supporting figure S8**). Removal of the N-terminal His-tagged SUMO did not affect the absorbance spectrum of YecA. Dialysis of YecA against buffer containing EDTA resulted in a decrease in absorbance at 330 nm (**figure 3B**), and the addition of an equimolar concentration of $FeSO_4$ restored absorbance of YecA at 330 nm (**figure 3B**). Taken together, these results suggested that the yellow colour of the purified YecA protein was due to coordination of Fe^{2+} (or potentially Fe^{3+}), and the slow conversion of the purified protein to colourless suggested that binding to iron was labile under the experimental conditions. Dialysis of YchJ against EDTA resulted in aggregation. Consequently, we did not investigate YchJ further.

EPR analysis of Fe^{3+} binding by YecA. To confirm that YecA can bind iron, we investigated the interaction of YecA with Fe^{3+} using EPR spectroscopy. The addition of a stoichiometric amount of purified metal-free YecA to a solution of Fe^{3+} (**figure 3C, blue line**) resulted in a new feature at 0.6145 T that is ~g = 4 (**figure 3C, red line**), indicating that there was a change in the electronic environment of the iron and indicating that YecA can bind to Fe^{3+}.

Identification of the iron-coordinating domain in YecA by NMR spectroscopy. To determine which domain was responsible for binding to iron, we purified ^{15}N- and ^{13}C-labelled YecA and investigated its structure using NMR spectroscopy. We could assign the resonances for the C-terminal 20 amino acids in the TROSY spectrum of the protein (excluding Pro-206 and Pro-208, which do not contain an N-H bond) (**figure 4A**). Several amino acids, including Arg-203, Asp-204, Asp-205, Leu-220 and His-221, produced two resonances, suggesting that the MBD in the metal-free protein exists in two distinct conformations (**figure 4A**). The addition of $FeSO_4$ resulted in the broadening and flattening of most of the resonances from amino acids in the MBD due to the paramagnetic properties of iron, but it affected very few of the resonances from the N-terminal ~200 amino acids (**figure 4B**). This result

bioRxiv preprint doi: https://doi.org/10.1101/613315; this version posted April 1, 2020. The copyright holder for this preprint (which was not certified by peer review) is the author/funder, who has granted bioRxiv a license to display the preprint in perpetuity. It is made available under aCC-BY-NC 4.0 International license.

suggested that the MBD is responsible for the iron-binding activity of YecA.

^{1}H-NMR analysis of metal binding by SecA-MBD. To investigate the relative affinity of the SecA MBD for zinc and iron, we examined binding of the SecA-MBD peptide to iron and zinc using ^{1}H-NMR. The addition of $ZnSO_4$ to SecA-MBD resulted in multiple changes in its ^{1}H-NMR spectrum including the appearance of resonances in the 8.5-9.5 ppm region, which are indicative of the formation of secondary structure (**figure 5A, blue and green traces**), consistent with previous studies (13). As with YecA, the addition of $FeSO_4$ resulted in a broadening and flattening of most of the ^{1}H resonances due to the paramagnetic properties of iron (**figure 5A, red trace**). The reduction in signal was more pronounced for ^{1}Hs that were nearer to the predicted metal binding site compared to those further away from the metal-binding site. $FeSO_4$ did not affect the spectra of control peptides that do not bind iron, indicating that the change in signal was caused by binding to iron.

We next investigated the ability of zinc to compete with iron for binding to SecA-MBD. To this end, we monitored the ^{1}H resonances from the valine methyl groups, which displayed differences that were distinctive for the apo-, Zn-bound and Fe-bound states (**figure 5B**). Previous work indicated that the dissociation rate of Zn^{2+} from the MBD is relatively rapid (half-life of minutes) (12). However, the addition of $ZnSO_4$ to SecA-MBD that had been pre-incubated with $FeSO_4$ did not cause a detectable change in the ^{1}H-NMR spectrum, even after ~40 minutes of incubation (**figure 5C**), suggesting that SecA-MBD binds preferentially to iron.

Role for a conserved serine in metal preference. The SecA MBD contains a nearly invariant serine residue, Ser-889 (**supporting figure S1**) (10,13), which is conserved in the MBD of YecA and both MBDs of YchJ (**supporting figure S9**). Previously published structural models of the SecA MBD indicate that the side chain of Ser-889 points inward toward the metal ligand and is not directly involved in binding to SecB (or likely ribosomes) (13,14,32) (**supporting figure S10**). In addition, the N-terminal MBD of YchJ, which lacks the amino acid residues required for binding to SecB, contains a serine at the same position suggesting that the serine is required for the structure of the MBD. In support of this notion, ^{1}H-NMR analysis indicated that SecA-MBD containing an alanine substitution at this position (SecA-MBD^{S889A}) exchanged iron for zinc at a detectable rate (**figure 5D**). These results suggested that Ser-889 is important for the folding of the MBD and/or coordination of the metal ion.

Binding affinity of SecA-MBD peptides for Zn^{2+}. To determine whether the alanine substitution caused a general defect in metal binding, we determined the affinity of SecA-MBD and SecA-MBD^{S889A} for Zn^{2+} using ITC. The affinity of the wild-type SecA-MBD for Zn^{2+} (36.0 ± 11.6 nM; **supporting figure S11A**) was not significantly different from that of SecA-MBD^{S889A} (46.0 ± 9.0 nM; **supporting figure S11B**), suggesting that the substitution does not affect its affinity for Zn^{2+}. We could not determine the affinity for SecA-MBD for iron due to the interfering heat exchange caused by aerobic oxidation of Fe^{2+} and because binding of SecA-MBD to Fe^{3+} did not cause a detectable heat exchange. Nonetheless, these results, taken together with the ^{1}H-NMR experiments, suggested that the serine-to-alanine substitution specifically affects the affinity of SecA-MBD^{S889A} for iron.

Modelling octahedral coordination of a metal by the SecA MBD. Because the strong reduction in signal in the ^{1}H-NMR spectrum of SecA-MBD caused by binding to iron made it difficult to determine the structure of the SecA MBD bound to iron directly, we modelled the structure of the MBD bound to iron using molecular dynamics. Fe^{2+} and Fe^{3+} can be hexavalent and are frequently coordinated in an octahedral geometry (33). We therefore simulated the MBD coordinated octahedrally to a hexavalent metal ion. In addition, we assumed that the hydroxyl group of Ser-889 and a hydroxyl ion from the solvent bound the two additional coordination sites of the metal. Finally, because it was not clear whether the δ- or ε-nitrogen of His-897 binds the metal, we simulated both possibilities. These simulations suggested that the imidazole ring of His-897 is out of plane with the metal ion (**figure 6**), and longer simulations using reduced constraints on the metal-coordinating atoms suggested that binding *via* the ε-nitrogen (**supporting figure S12A**) was more stable than *via* the δ-nitrogen (**supporting figure S12B**), consistent with the structures of other iron-binding proteins (34). Tetrahedral coordination of zinc was previously reported to induce strain into the polypeptide backbone (13). However,

bioRxiv preprint doi: https://doi.org/10.1101/613315; this version posted April 1, 2020. The copyright holder for this preprint (which was not certified by peer review) is the author/funder, who has granted bioRxiv a license to display the preprint in perpetuity. It is made available under aCC-BY-NC 4.0 International license.

Ramachandran plots of the structures generated by our simulations indicated that the MBD can coordinate iron octahedrally without inducing stress in the polypeptide backbone (**supporting data S3 and S4**). The SecB-binding surface was not significantly perturbed in the iron-bound structural models compared to previously published structures (**supporting data S3 and S4**) (13,14). These results indicate that Ser-889 can participate in coordination of a hexavalent metal, such as iron.

DISCUSSION

Our results indicate that iron is a physiological ligand of SecA-like MBDs. The SecA CTT, YecA and YchJ copurify with significant amounts of iron, and full-length SecA copurifies predominantly with iron when rapidly purified from cells producing it at low levels. Biophysical experiments indicate that the MBDs of SecA and YecA can bind to iron, and competition experiments suggest that the MBD of SecA binds preferentially to iron. Finally, our results indicate that azide treatment causes autoinhibition of SecA *in vivo* by disrupting the interaction of the MBD with iron. Taken together, our results suggest that a significant proportion of SecA is bound to iron *in vivo* and that the iron-bound form could play a physiological role in regulating the activity of the protein.

Our results do not exclude the possibility that both iron and zinc are physiological ligands of the MBD. For example, it is possible that the relative abundances of the zinc- and iron-bound forms of SecA are involved in autoregulation of SecA by the CTT. Indeed, the Zn-bound form of the protein appears to be functional *in vitro* (12,14,35,36). However, the known abundances of zinc and iron in the cell suggest that the iron-bound form of SecA is the dominant species *in vivo*. Although the affinity of the SecA-MBD-iron complex could not be determined directly, the preference of the MBD for iron over zinc suggests that the K_D is less than 40 nM. The cytoplasmic concentration of iron is normally ~50 nM while the concentration of free zinc is fM to pM (33,37,38). In addition, although metal-binding proteins bind promiscuously to different transition metals, they typically bind with higher affinity to zinc than to iron (33,38), making the higher affinity of the SecA MBD for iron remarkable. These results suggest that the MBD is normally bound to iron *in vivo*. The strong conservation of Ser-889 suggests that iron binding is evolutionarily conserved.

Our molecular dynamics simulations suggest that the specificity of the MBD for iron could be determined by the binding geometry. Zinc is nearly always bound using a tetrahedral geometry while iron can be coordinated using several geometries, including octahedral (33,38). Previous work has established that Cys-885, Cys-887, Cys-896 and His-897 are required for binding to metal (12,14). Our experimental results suggest the conserved serine also participates in coordination of the bound metal ion, suggesting that the bound metal ion is coordinated using at least five sites. It is not yet clear if the bound iron is coordinated at a sixth site and if so, which amino acid binds the iron. Our simulations used a solvent molecule to coordinate the bound metal, but it is possible that the conserved aromatic residue at position 893 indirectly participates in coordination of the metal (13). For example, the π-ring system of Tyr-893 could coordinate a solvent molecule that participates in metal-ion coordination (39). Although π-electron systems can coordinate iron (40), preliminary simulations suggest that binding of Tyr-893 to the metal results in steric clashes with the other metal-coordinating side-chains.

Our results provide a potential explanation for the discrepancy between the concentrations of azide required to inhibit SecA *in vivo* and *in vitro*. Previous work indicates that azide binds to the ADP-bound form of SecA and inhibits nucleotide exchange (19,20). Our results suggest that azide additionally disrupts the structure of the iron-bound MBD, resulting in autoinhibition of SecA. Our results suggest that SecA detaches from the cytoplasmic membrane as a consequence of disrupting the MBD. Previous research indicates that CTT-mediated autoinhibition is not sufficient to completely inhibit growth of *E. coli* (10,35). However, our results suggest that autoinhibition slows bacterial growth at subinhibitory concentrations of azide, which likely enhances the inhibitory effect of azide on the ATPase activity of SecA at inhibitory concentrations. We cannot rule out the possibility that the role of the bound iron ion is purely structural. Indeed, many helicases contain evolutionarily conserved iron-sulfur clusters that appear to function solely as structural scaffolds (41). However, our results raise the possibility that the MBD senses an environmental stress and that

bioRxiv preprint doi: https://doi.org/10.1101/613315; this version posted April 1, 2020. The copyright holder for this preprint (which was not certified by peer review) is the author/funder, who has granted bioRxiv a license to display the preprint in perpetuity. It is made available under aCC-BY-NC 4.0 International license.

azide treatment mimics this stress. For example, the MBD could sense changes in the oxidation state of the bound iron (Fe^{2+} versus Fe^{3+}), the identity of the bound metal (Zn versus Fe) or the oxidation state of the metal coordinating cysteines (42-44).

The functions of YecA and YchJ are unknown. Both proteins contain domains of unknown function (UPF0149 in YecA and UPF0225 in YchJ (45)) and are found in a broad range of bacterial species. Neither protein is universally conserved (31) or essential for viability (23,46). However, the conservation of the amino acids that mediate the interaction between the SecA MBD and SecB in the C-terminal MBDs of YecA and YchJ suggest that that these proteins could also potentially interact with the SecB or ribosomes. Large scale genetic screens do not suggest an obvious function for either proteins (46,47), suggesting that YecA and YchJ do not carry out their functions under laboratory growth conditions or are not normally produced (or both). The sole publication mentioning *yecA* (48) suggests that it could encode the gene *ssaG* (*ssa* mutants suppress the temperature sensitive growth defect caused by a *secA51* mutation) (49). However, whole genome sequencing of strain DO314 (which contains an *ssaG1* mutation) suggests that the suppressor mutation does not map to the *yecA* gene (unpublished result).

The evolutionary conservation of the MBD supports the idea that YecA and YchJ interact with the ribosome. In addition to recent work suggesting that MBD of SecA binds to the ribosome (10), the methionine amino peptidases of many bacterial species contain a SecA-like MBD (45). (In *E. coli*, methionine amino peptidase binds to the ribosome (50).) In addition, ribosomal protein L35a in *Drosophila melanogaster* contains a SecA-like MBD, suggesting that this role is evolutionarily conserved. Our results suggest that SecA-like MBDs could also regulate interactions with the ribosome in response to environmental stress.

EXPERIMENTAL PROCEDURES

Chemicals and media. All chemicals were purchased from Fisher or Sigma-Aldrich unless indicated. Synthetic peptides were synthesised by Severn Biotech (Kidderminster, UK) or using an in-house synthesiser. The quality of the peptides was checked using MALDI mass spectrometry. 100X EDTA-free protease inhibitor cocktail was purchased from Pierce (Thermo-Fisher). Cells were grown using LB medium (51). Where indicated, IPTG was added to the culture medium. Where required, kanamycin (30 μg/ml) was added to the growth medium.

Strains and plasmids. Strains and plasmids were constructed using common genetic methods (51). Single gene deletion mutants from the Keio collection (46) were obtained from the *E. coli* genetic stock centre (CGSC; Yale University, New Haven, Connecticut). Strain MG1115 (52) was a kind gift from M. Grabowicz and T. Silhavy. Strain DO314 (which contains an *ssaG1* mutation) was a kind gift from D. Oliver. All other strains were lab stocks.

Azide sensitivity assays. Filter disc assays were conducted as described by Huie and Silhavy (17) except that bacterial lawns were produced by evenly swabbing an overnight culture of *E. coli* over the surface of an LB containing the indicated concentrations of EDTA, $ZnSO_4$ or $FeSO_4$. An empty 6 mm antibiotic assay filter disc (Merck-Millipore) was then placed in the centre of the lawn and 10 μl of 1 M NaN_3 was pipetted onto the filter disc. The lawns were then grown overnight at 37°C.

TraDIS. TraDIS experiments were conducted as described previously (22,23). 50 ml of LB broth containing 0, 0.25 or 0.5 mM NaN_3 were inoculated with 10 μl of a library of ~1 million *E. coli* BW25113 mini-Tn5 insertion mutants, and the cultures were grown to OD_{600} 1.0. Genomic DNA was extracted using a Qiagen QIAamp DNA blood mini kit and then processed using a two-step PCR method (53), which results in Illumina-compatible products. The PCR products were purified using the Agencourt AMPure XP system by Beckman Coulter. The products were sequenced using an Illumina MiSeq sequencer and the reads were mapped to the *E. coli* reference genome NC_007779.1 (*E. coli* K-12 substr. W3110). The number of insertions in the coding sequences (CDS) for each gene was then determined. To reduce the number of false positives due to sequencing assignment errors, genes that exist in multiple copies on the chromosome (e.g. insertion elements and rRNA operons) were eliminated from the analysis**.** Genes containing 15 or fewer total insertions across all three conditions were eliminated in the data presented in **figure 1A**.

Phospholipid binding assay. Strains producing His-SUMO-SecA (DRH625; (53)) or

bioRxiv preprint doi: https://doi.org/10.1101/613315; this version posted April 1, 2020. The copyright holder for this preprint (which was not certified by peer review) is the author/funder, who has granted bioRxiv a license to display the preprint in perpetuity. It is made available under aCC-BY-NC 4.0 International license.

His-SUMO- SecA$^{C885A/C887A}$ (MJ118; (10)) were grown to late log phase in LB and induced using 1 mM IPTG. For *in vivo* experiments, the culture was divided after the addition of IPTG, and half of the culture was treated with 2 mM sodium azide for 10 minutes. Cells were harvested by centrifugation, resuspended in lysis buffer (20 mM HEPES [potassium salt] pH 7.5, 500 mM NaCl, 1 mM tris(2-carboxyethyl)phosphine [TCEP]) and lysed by cell disruption. Clarified cell lysates were passed over a 1 ml Ni-HiTrap column (GE Biosciences), and the bound protein was washed with 50 volumes of lysis buffer containing 20 mM Imidazole. His-SUMO-SecA was eluted from the column using lysis buffer containing 500 mM imidazole and dialysed against wash buffer lacking imidazole. The concentration of the protein was adjusted to 1 mg/ml to a final volume of 2 ml, and the phospholipids were extracted using 2 ml methanol and 1 ml chloroform. The chloroform phase was removed, and phospholipids were concentrated by air drying and resuspending in chloroform to a final volume of 100 µl. The indicated volume of sample was spotted onto TLC silica gel 60 T_{254} plates (Merck Millipore) and resolved using a mixture of 60 chloroform: 25 methanol: 4 water. For the *in vitro* phospholipid release assay, 0.2 mg of His-SUMO-SecA purified from untreated cells was bound to 100 µl Ni-NTA agarose beads (Life Technologies). The beads were incubated with 500 µl of lysis buffer or buffer containing 2 mM sodium azide for 10 minutes and washed three times with 500 µl lysis buffer. The protein was eluted from the beads with lysis buffer containing 500 mM imidazole, and the phosopholipid content of the supernatant was analysed using the method described above.

Determination of metal content of Strep-SUMO-CTT. To determine the effect of azide on binding of Strep-SUMO-CTT to iron, 100 ml cultures of BL21(DE3) containing plasmid pDH543 (10) were grown to OD_{600} 1.0 in LB, and production of Strep-SUMO-CTE was induced using 1 mM IPTG. After 1 hour, cultures were split, and half the culture was treated with 2 mM NaN_3 for 10 minutes. Cells were rapidly cooled, harvested by centrifugation and lysed using B-PER cell lysis reagent from Pierce (Rockford, Illinois). Cell lysates were incubated for 15 minutes with 50 µl of a 50% Streptactin-Sepharose slurry that had been pre-equilibrated with wash buffer (10 mM HEPES (potassium salt) pH 7.5, 100 mM potassium acetate) and washed extensively with wash buffer. The samples were washed a final time using 10 mM HEPES (potassium salt) pH 7.5 to remove excess salt, and the total protein was eluted off of the column using using 10 mM HEPES (potassium salt) pH 7.5 buffer containing 7M guanidinium hydrochloride. The propensity to aggregate was determined by diluting 50 µl of the guanidinium-denatured protein into 950 µl of a 20 mM HEPES buffer and measuring light scattering at 500 nm. The metal content of the samples was determined using ICP-MS (School of Geography, Earth and Environmental Sciences, University of Birmingham, UK).

Determination of metal content of SecA-biotin. 100 ml cultures of DRH839 (MC4100 Δ*secA* λ-p_{trc}-*secA-biotin*..SpecR) (30) were grown in 10 µM or 100 µM IPTG to OD_{600} ~ 1. Cells were lysed using cell disruption, and lysates were incubated with 100 µl Streptactin-sepharose (IBA Lifesciences, Göttingen, Germany) for 15 minutes. The beads were washed four times with 30 ml buffer (50 mM potassium HEPES, pH 7.5, 100 mM potassium acetate, 10 mM magnesium acetate, 0.1% nonidet P40). Metal was eluted from the beads by incubating with 10 mM HEPES, pH 7.5, 50 mM EDTA) at 55˚C for 30 minutes, and the zinc and iron content was determined using ICP-OES. The amount of bound protein was determined by boiling in SDS sample buffer and analysing using Bradford reagent (BioRad, Hercules, CA). The eluted protein was resolved on a BioRad 15% TGX gel. The metal content was determined using ICP-OES (School of Geography, Earth and Environmental Sciences, University of Birmingham, UK).

Purification of YecA and YchJ. The *yecA* and *ychJ* genes from *Escherichia coli* K-12 were fused in-frame to the 3′ end of the gene encoding SUMO from *S. cerevisiae* in plasmid pCA528 and purified as described previously (54). For identification of the copurifying metals and absorbance spectroscopy, BL21(DE3) cells containing the SUMO-YecA and SUMO-YchJ plasmids were grown to OD_{600} 1.0 at 37°C. Cells were then shifted to 25°C and grown overnight in the presence of 1 mM IPTG. Cells were lysed in buffer 1 (20 mM potassium HEPES, pH 7.5, 100 mM potassium acetate, 10 mM magnesium acetate) containing protease inhibitor by cell disruption.

bioRxiv preprint doi: https://doi.org/10.1101/613315; this version posted April 1, 2020. The copyright holder for this preprint (which was not certified by peer review) is the author/funder, who has granted bioRxiv a license to display the preprint in perpetuity. It is made available under aCC-BY-NC 4.0 International license.

When noted, TCEP was added to buffer 1 during lysis at a concentration of 1 mM. Lysates were passed over a 1 ml His-Trap HF column (GE Healthcare). The bound protein was washed with 15 ml high salt wash buffer (20 mM potassium HEPES, pH 7.5, 500 mM potassium acetate, 10 mM magnesium acetate, 50 mM imidazole and 15 ml low salt wash buffer (20 mM potassium HEPES, pH 7.5, 100 mM potassium acetate, 10 mM magnesium acetate, 50 mM imidazole). The bound protein was eluted using elution buffer (20 mM potassium HEPES, pH 7.5, 100 mM potassium acetate, 10 mM magnesium acetate, 500 mM imidazole). The eluted protein was dialysed against buffer 1 to remove the imidazole and concentrated using concentrators with a 5 kDa cutoff (Vivaspin).

For HSQC-NMR analysis of YecA, cells containing the YecA plasmid were grown in M9 minimal media containing $^{15}NH_4Cl$, $^{1}H_7$-$^{13}C_6$-glucose (2 g/l) and trace minerals. Cultures were grown to OD_{600} 0.8 at 37°C, shifted to 18°C and induced overnight with 1 mM IPTG. Cells were lysed by cell disruption and purified using a 1 ml His-Trap column as described above. After elution, the protein was treated with purified hexahistidine-tagged Ulp1 from *S. cerevisiae* to remove the SUMO tag and dialysed overnight against buffer 2 (20 mM potassium HEPES, pH 7.5, 100 mM potassium acetate, 10 mM magnesium acetate, 5 mM β-mercaptoethanol) to remove the imidazole. The SUMO tag and Ulp1 protease were removed from the purified protein by passing the cut protein over a 1 ml His-Trap column. Purified YecA was then concentrated using anion exchange chromatography, and the eluate was dialyzed against buffer 3 (20 mM potassium HEPES, pH 7.5, 100 mM potassium acetate, 10 mM magnesium acetate, 5 mM β-mercaptoethanol, 1 mM EDTA) and finally against buffer 1 to remove the β-mercaptoethanol and EDTA.

Metal ion analysis. The metal ion content of purified YecA and YchJ was determined using ICP-MS (School of GEES, University of Birmingham). The 5 kDa MWCO concentrator filtrate (Sartorius, Göttingen, Germany) was used to control for the amount of unbound metal in the protein samples. The zinc and iron ion content of the EDTA eluate from the Ni-NTA column after purification in the presence of 1 mM TCEP was determined using ICP-OES (School of Geography, Earth and Environmental Sciences, University of Birmingham).

Absorbance spectroscopy. The absorbance spectra of 200 µl of 600-800 µM purified YecA or YchJ in buffer 1 were determined from 300-600 nm using a CLARIOstar plate reader (BMG Labtech) using UV-clear flat bottomed 96-well plates (Greiner). The absorbance spectrum for the buffer alone was subtracted from that of the purified protein, and the absorbance was normalised to the concentration of the protein in the sample.

EPR spectroscopy. EPR samples were suspended in 50 µl buffer 1 containing 30% glycerol. For YecA, samples contained 0.85 mM $FeCl_3$ or 0.6 mM YecA and $FeCl_3$. For SecA-MBD, samples contained 0.5 mM $FeSO_4$, which had been left to oxidize aerobically in a 25 mM water/glycerol stock, with 0.5 mM SecA-MBD or just the metal salt in buffer. Measurements were taken with a Bruker Elexsys E580 spectrometer with an ER 5106QT-2w cylindrical resonator operating at 34 GHz, i.e. Q-band. Quartz tubes with 3 mm O.D. were used. Experiments were conducted at 10 K using a cryogen free variable temperature cryostat (from Cryogenic Limited). Echo-detected field sweeps were conducted by sweeping from 0.1 to 1.7 T with 4000 points using a Hahn echo sequence where the π pulse length was 32 ns and the time between pulses was 400 ns. The power level was determined by observing the maximum echo and was around 0.38 mW which is indicative of a high-spin system. The shot repetition time was set at 100 µs with 50 shots per point which was sufficient for the iron, though caused some saturation of the Mn^{2+} contaminant peak. The resultant echo-detected field swept profiles were normalised for plotting, taking account of differences in video gain, concentration and numbers of averages.

NMR backbone assignment of YecA. Assignment spectra were acquired on 0.5 mM ^{15}N, ^{13}C-labelled protein in 20 mM [MES]-NaOH [pH 6.0], 10 mM NaCl, 10% D_2O in a 5 mm Shigemi tube (Shigemi Inc.). The ^{1}H, ^{15}N, and ^{13}C resonances of the YecA backbone were assigned using BEST TROSY versions of HNCA, HN(CO)CA, HNCACB, HN(CO)CACB, HNCO and HN(CA)CO (55-61). All experiments were performed at 298 K and acquired with a spectral width of 14 ppm in ^{1}H , collecting 1024 real data points, and 30 ppm in ^{15}N, collecting 92 increments

bioRxiv preprint doi: https://doi.org/10.1101/613315; this version posted April 1, 2020. The copyright holder for this preprint (which was not certified by peer review) is the author/funder, who has granted bioRxiv a license to display the preprint in perpetuity. It is made available under aCC-BY-NC 4.0 International license.

using a Bruker 900 MHz spectrometer equipped with a 4-channel AVANCE III HD console and a 5 mm TCI z-PFG cryogenic probe The centre of the spectra was set to 4.698 ppm in the ^{1}H and 118 ppm in ^{15}N. All spectra were acquired collecting 128 increments in the ^{13}C dimension using a non-uniform sampling scheme. The HN(CO)CACB and HNCACB experiments were acquired using 64 scans per increment, a spectral width of 76 ppm in the ^{13}C direction with the centre around 43.665 ppm. The HNCA and the HN(CO)CA experiments were acquired using 32 scans per increment, a ^{13}C spectral width of 30 ppm with the centre of the spectra set to 55.9 ppm. The HN(CA)CO and HNCO experiments were acquired using 32 scans per increment, a ^{13}C spectral width of 16 ppm centred around 176.2 ppm. Non-uniformed sampled data were reconstructed using the compressed sensing algorithm with MDDNMR (62) and processed using nmrPipe (63). Spectra were analysed in Sparky (64).

^{1}H-NMR spectroscopy. All spectra were obtained at 298 K on a Bruker 900 MHz spectrometer equipped with a cryogenically cooled 5 mm TCI probe using excitation sculpting for water suppression on a sample in 90% H_2O/10% D_2O. Sequence specific assignments were completed using a TOCSY experiment in 90% H_2O/10% D_2O using a DIPSI2 spin-lock with a mixing time of 65 ms, 32 transients and collecting 512 increments with a spectral width of 10 ppm in both dimensions. 1D data sets comprised 16 transients, 32000 data points and a spectral width of 16 ppm. All data were processed using Topspin 3.2.6 software using an exponential window function with a line broadening of 1 Hz.

ITC. ITC measurements were conducted in a MicroCal VP-ITC calorimeter (Piscataway, NJ, USA). All solutions were centrifuged for 5 min at 13,000 rpm and then thoroughly degassed under vacuum for 5 min with gentle stirring immediately before use. 0.1 mM $ZnSO_4$ was titrated into a solution of the indicated peptide (0.01 mM) in the sample cell (Vo = 1.4037 ml). Titrations consisted of a preliminary 2 µl injection followed by 50 6 µl injections of 12 s duration with 700 s between each injection. All experiments were conducted at 25˚C with an initial reference power of 10 µcal/s. The raw data were analysed with Origin 7.0 using one-binding site model and were corrected for the heat of dilution of the metal ion in the absence of peptide.

Molecular dynamics simulations. Energy minimisations and molecular dynamics simulations were performed using Amber 18 (65). All parameters were from the Amber force field ff14SB (66), except where noted below. Charges for the deprotonated serine (renamed SEO) were determined by comparison with deprotonated cysteine (Amber residue name CYM) (**supporting table S2)**. Parameters for the Fe^{2+} bound histidine (His 897) and HO- were as previously described (67). An SPCE water model and a 2+ iron ion were used, as previously described (68-71). The C-terminal 24 amino acids of SecA (KVGRNDPCPCGSGKKYKQCHGRLQ) were used for modelling. Initial molecular coordinates were derived from the superposition of structures 1SX1 (13) (residues 1 to 21) and 1TM6 (32), followed by energy minimisation, to remove any strain arising from the fusing of the two coordinate sets. The system was then solvated in an octahedral box of water extending 8 Å from the protein surface. Ewald summation was applied to the simulations with a non-bonded cut-off of 10 Å. The system was minimised with positional restraints (500 kcal/(mol•Å)) on every atom of the peptide and on the iron. This was followed by further minimisation without positional restraints but with weak restraints to enforce an octahedral geometry. Distance restraints were applied between the iron and the six chelating atoms (10 kcal/(mol•Å)), as indicated in the legend of **figure S7**, and between atoms on adjacent vertices of the octahedron, listed in **supporting table S4** (2.5 kcal/(mol•Å)). A torsion angle restraint (10 kcal/(mol•rad)) was applied to the sulfur atoms of the residues Cys885, Cys887 and Cys896 and to the δ or ε nitrogens of His897. **Supporting table S3** presents a list of all the restraint parameters. The system was then heated to 300 K in six 50 K steps, using an NVT ensemble and a Langevin thermostat with $\gamma = 1\ \mathrm{ps}^{-1}$. The peptide and iron were subjected to positional restraints (10 kcal/(mol•Å)), but no other restraints, during the entire heating process. Subsequently, the system was equilibrated for 1.2 ns using an NPT ensemble and a Langevin

bioRxiv preprint doi: https://doi.org/10.1101/613315; this version posted April 1, 2020. The copyright holder for this preprint (which was not certified by peer review) is the author/funder, who has granted bioRxiv a license to display the preprint in perpetuity. It is made available under aCC-BY-NC 4.0 International license.

thermostat with $\gamma = 1\ \mathrm{ps}^{-1}$. Residues directly involved in the octahedral coordination of iron had a constant positional restraint of 10 kcal/(mol•Å) applied for 600 ps, followed by application of the distance and torsional restraints previously defined. Residues not directly chelated to the iron also had positional restraints initially of 10 kcal/(mol•Å), but reduced to 1 kcal/(mol•Å) at 200ps, 0.1 kcal/(mol•Å)) at 400 ps and zero from 600 ps onwards. A 100 ns long production simulation was performed in an NPT ensemble with a Berendsen thermostat ($\tau = 10\ \mathrm{ps}$). The same distance and torsional restraints were applied as described for the minimisation. This 100 ns simulation was then extended for a further 20 ns, for a total of 120 ns, but with the force constants reduced from 10 to 2 kcal/(mol•Å), 2.5 to 0.5 kcal/(mol•Å) and 10 to 2 kcal/(mol•rad) for distances between iron and chelating atoms, distances between adjacent atoms on the surface of the octahedron and torsion angle, respectively. The above protocol was followed once with the restraints between His-897 and iron via the δ-N and once with the restraints via the ε-N.

bioRxiv preprint doi: https://doi.org/10.1101/613315; this version posted April 1, 2020. The copyright holder for this preprint (which was not certified by peer review) is the author/funder, who has granted bioRxiv a license to display the preprint in perpetuity. It is made available under aCC-BY-NC 4.0 International license.

DATA AVAILABILITY STATEMENT

HSQC and ^{1}H-NMR were deposited in the Biological Magnetic Resonance Databank under accession 27881. EPR data is available at doi: 10.17630/11b18167-18c0-42ae-a54c-1fe09432e91f. BED files of the TraDIS sequencing data are available at doi: 10.6084/m9.figshare.5280733. All other data has been published in the manuscript or as supporting information.

ABBREVIATIONS

BEST, band-selective short transient excitation; DIPSI, decoupling in the presence of scalar interactions; DTT, dithiothreitol; EDTA, ethylene diamine tetra-acetic acid; EPR, electron paramagnetic resonance; HSQC, heteronuclear single quantum coherence; ICP, inductively coupled plasma; IPTG, isopropyl-β-thiogalactoside; ITC, isothermal titration calorimetry; MS, mass spectrometry; NMR, nuclear magnetic resonance; NTA, nitrilotriacetic acid; OES, optical emission spectrometry; SUMO, small ubiquitin-like modifier; TCEP, tris(2-carboxyethyl)phosphine; TOCSY, total correlated spectroscopy; TROSY, transverse relaxation optimised spectroscopy; UPF, unidentified protein function; UV, ultraviolet

ACKNOWLEDGEMENTS

We thank J. Cole, J. Green, A. Peacock and O. Daubney for advice and assistance. We thank Drs C. Stark, S. Baker, M. Thompson, H. El Mkami and A. Shah for technical assistance and members of the Henderson, Lund and Grainger labs for insightful discussions. TCS was funded by the Biotechnology and Biological Sciences Research Council (BBSRC) Midlands Integrated Integrative Biosciences Training Partnership (MIBTP). MA was funded by Jouf University. DH and MJ were funded by BBSRC grant BB/L019434/1. TK was funded by BBSRC grant BB/P009840/1. EHAA was supported by the Ministerio de Ciencia, Tecnología e Innovación del govierno de Colombia and the British Council. JEL thanks the Royal Society for a University Research Fellowship and the Wellcome Trust for the Q-band EPR spectrometer (099149/Z/12/Z). NMR work was supported by the Wellcome Trust (099185/Z/12/Z), and we thank HWB-NMR at the University of Birmingham for providing open access to their Wellcome Trust-funded 900 MHz spectrometer.

CONFLICTS OF INTEREST

The authors declare that they have no conflicts of interest with the contents of this article.

REFERENCES

1. Beckwith, J. (2013) The Sec-dependent pathway. *Research in microbiology* **164**, 497-504
2. Tsirigotaki, A., De Geyter, J., Sostaric, N., Economou, A., and Karamanou, S. (2017) Protein export through the bacterial Sec pathway. *Nat Rev Microbiol* **15**, 21-36
3. Park, E., and Rapoport, T. A. (2012) Mechanisms of Sec61/SecY-mediated protein translocation across membranes. *Annu Rev Biophys* **41**, 21-40
4. Cranford Smith, T., and Huber, D. (2018) The way is the goal: how SecA transports proteins across the cytoplasmic membrane in bacteria. *FEMS Microbiol Lett* **365**
5. Collinson, I., Corey, R. A., and Allen, W. J. (2015) Channel crossing: how are proteins shipped across the bacterial plasma membrane? *Philos Trans R Soc Lond B Biol Sci* **370**
6. Matsuyama, S., Kimura, E., and Mizushima, S. (1990) Complementation of two overlapping fragments of SecA, a protein translocation ATPase of Escherichia coli, allows ATP binding to its amino-terminal region. *J Biol Chem* **265**, 8760-8765
7. Or, E., Boyd, D., Gon, S., Beckwith, J., and Rapoport, T. (2005) The bacterial ATPase SecA functions as a monomer in protein translocation. *J Biol Chem* **280**, 9097-9105
8. Or, E., Navon, A., and Rapoport, T. (2002) Dissociation of the dimeric SecA ATPase during protein translocation across the bacterial membrane. *Embo J* **21**, 4470-4479
9. Shinkai, A., Akita, M., Matsuyama, S., and Mizushima, S. (1990) Quantitative renaturation from a guanidine-denatured state of the SecA dimer, a 200 KDa protein involved in protein secretion in Escherichia coli. *Biochem Biophys Res Commun* **172**, 1217-1223

bioRxiv preprint doi: https://doi.org/10.1101/613315; this version posted April 1, 2020. The copyright holder for this preprint (which was not certified by peer review) is the author/funder, who has granted bioRxiv a license to display the preprint in perpetuity. It is made available under aCC-BY-NC 4.0 International license.

10. Jamshad, M., Knowles, T. J., White, S. A., Ward, D. G., Mohammed, F., Rahman, K. F., Wynne, M., Hughes, G. W., Kramer, G., Bukau, B., and Huber, D. (2019) The C-terminal tail of the bacterial translocation ATPase SecA modulates its activity. *eLife* **8**
11. Gelis, I., Bonvin, A. M., Keramisanou, D., Koukaki, M., Gouridis, G., Karamanou, S., Economou, A., and Kalodimos, C. G. (2007) Structural basis for signal-sequence recognition by the translocase motor SecA as determined by NMR. *Cell* **131**, 756-769
12. Fekkes, P., de Wit, J. G., Boorsma, A., Friesen, R. H., and Driessen, A. J. (1999) Zinc stabilizes the SecB binding site of SecA. *Biochemistry* **38**, 5111-5116
13. Dempsey, B. R., Wrona, M., Moulin, J. M., Gloor, G. B., Jalilehvand, F., Lajoie, G., Shaw, G. S., and Shilton, B. H. (2004) Solution NMR structure and X-ray absorption analysis of the C-terminal zinc-binding domain of the SecA ATPase. *Biochemistry* **43**, 9361-9371
14. Zhou, J., and Xu, Z. (2003) Structural determinants of SecB recognition by SecA in bacterial protein translocation. *Nat Struct Biol* **10**, 942-947
15. Oliver, D. B., Cabelli, R. J., Dolan, K. M., and Jarosik, G. P. (1990) Azide-resistant mutants of Escherichia coli alter the SecA protein, an azide-sensitive component of the protein export machinery. *Proc Natl Acad Sci U S A* **87**, 8227-8231
16. Fortin, Y., Phoenix, P., and Drapeau, G. R. (1990) Mutations conferring resistance to azide in Escherichia coli occur primarily in the secA gene. *J Bacteriol* **172**, 6607-6610
17. Huie, J. L., and Silhavy, T. J. (1995) Suppression of signal sequence defects and azide resistance in Escherichia coli commonly result from the same mutations in secA. *J Bacteriol* **177**, 3518-3526
18. Chun, S. Y., and Randall, L. L. (1994) In vivo studies of the role of SecA during protein export in Escherichia coli. *J Bacteriol* **176**, 4197-4203
19. Bowler, M. W., Montgomery, M. G., Leslie, A. G., and Walker, J. E. (2006) How azide inhibits ATP hydrolysis by the F-ATPases. *Proc Natl Acad Sci U S A* **103**, 8646-8649
20. Schmidt, M., Ding, H., Ramamurthy, V., Mukerji, I., and Oliver, D. (2000) Nucleotide binding activity of SecA homodimer is conformationally regulated by temperature and altered by prlD and azi mutations. *J Biol Chem* **275**, 15440-15448
21. van der Wolk, J. P., de Wit, J. G., and Driessen, A. J. (1997) The catalytic cycle of the escherichia coli SecA ATPase comprises two distinct preprotein translocation events. *EMBO J* **16**, 7297-7304
22. Langridge, G. C., Phan, M. D., Turner, D. J., Perkins, T. T., Parts, L., Haase, J., Charles, I., Maskell, D. J., Peters, S. E., Dougan, G., Wain, J., Parkhill, J., and Turner, A. K. (2009) Simultaneous assay of every Salmonella Typhi gene using one million transposon mutants. *Genome research* **19**, 2308-2316
23. Goodall, E. C. A., Robinson, A., Johnston, I. G., Jabbari, S., Turner, K. A., Cunningham, A. F., Lund, P. A., Cole, J. A., and Henderson, I. R. (2018) The Essential Genome of Escherichia coli K-12. *MBio* **9**
24. Lill, R., Dowhan, W., and Wickner, W. (1990) The ATPase activity of SecA is regulated by acidic phospholipids, SecY, and the leader and mature domains of precursor proteins. *Cell* **60**, 271-280
25. Cabelli, R. J., Dolan, K. M., Qian, L. P., and Oliver, D. B. (1991) Characterization of membrane-associated and soluble states of SecA protein from wild-type and SecA51(TS) mutant strains of Escherichia coli. *J Biol Chem* **266**, 24420-24427
26. Ulbrandt, N. D., London, E., and Oliver, D. B. (1992) Deep penetration of a portion of Escherichia coli SecA protein into model membranes is promoted by anionic phospholipids and by partial unfolding. *J Biol Chem* **267**, 15184-15192
27. Breukink, E., Demel, R. A., de Korte-Kool, G., and de Kruijff, B. (1992) SecA insertion into phospholipids is stimulated by negatively charged lipids and inhibited by ATP: a monolayer study. *Biochemistry* **31**, 1119-1124

bioRxiv preprint doi: https://doi.org/10.1101/613315; this version posted April 1, 2020. The copyright holder for this preprint (which was not certified by peer review) is the author/funder, who has granted bioRxiv a license to display the preprint in perpetuity. It is made available under aCC-BY-NC 4.0 International license.

28. Bauer, B. W., Shemesh, T., Chen, Y., and Rapoport, T. A. (2014) A "push and slide" mechanism allows sequence-insensitive translocation of secretory proteins by the SecA ATPase. *Cell* **157**, 1416-1429
29. Breukink, E., Nouwen, N., van Raalte, A., Mizushima, S., Tommassen, J., and de Kruijff, B. (1995) The C terminus of SecA is involved in both lipid binding and SecB binding. *J Biol Chem* **270**, 7902-7907
30. Huber, D., Jamshad, M., Hanmer, R., Schibich, D., Doring, K., Marcomini, I., Kramer, G., and Bukau, B. (2017) SecA Cotranslationally Interacts with Nascent Substrate Proteins In Vivo. *J Bacteriol* **199**
31. The UniProt, C. (2017) UniProt: the universal protein knowledgebase. *Nucleic Acids Res* **45**, D158-D169
32. Matousek, W. M., and Alexandrescu, A. T. (2004) NMR structure of the C-terminal domain of SecA in the free state. *Biochim Biophys Acta* **1702**, 163-171
33. Waldron, K. J., Rutherford, J. C., Ford, D., and Robinson, N. J. (2009) Metalloproteins and metal sensing. *Nature* **460**, 823-830
34. Chakrabarti, P. (1990) Geometry of Interaction of Metal-Ions with Histidine-Residues in Protein Structures. *Protein Engineering* **4**, 57-63
35. Fekkes, P., van der Does, C., and Driessen, A. J. (1997) The molecular chaperone SecB is released from the carboxy-terminus of SecA during initiation of precursor protein translocation. *Embo J* **16**, 6105-6113
36. Fekkes, P., de Wit, J. G., van der Wolk, J. P., Kimsey, H. H., Kumamoto, C. A., and Driessen, A. J. (1998) Preprotein transfer to the Escherichia coli translocase requires the co-operative binding of SecB and the signal sequence to SecA. *Mol Microbiol* **29**, 1179-1190
37. Osman, D., Martini, M. A., Foster, A. W., Chen, J., Scott, A. J. P., Morton, R. J., Steed, J. W., Lurie-Luke, E., Huggins, T. G., Lawrence, A. D., Deery, E., Warren, M. J., Chivers, P. T., and Robinson, N. J. (2019) Bacterial sensors define intracellular free energies for correct enzyme metalation. *Nature Chemical Biology*
38. Waldron, K. J., and Robinson, N. J. (2009) How do bacterial cells ensure that metalloproteins get the correct metal? *Nat Rev Microbiol* **7**, 25-35
39. Zaric, S. D., Popovic, D. M., and Knapp, E. W. (2000) Metal ligand aromatic cation-pi interactions in metalloproteins: Ligands coordinated to metal interact with aromatic residues. *Chem-Eur J* **6**, 3935-3942
40. Marty, P., Serra, G., Chaudret, B., and Ristorcelli, I. (1994) Iron Aromatics Coordination in Molecular Clouds. *Astron Astrophys* **282**, 916-923
41. White, M. F., and Dillingham, M. S. (2012) Iron-sulphur clusters in nucleic acid processing enzymes. *Curr Opin Struct Biol* **22**, 94-100
42. Jakob, U., Eser, M., and Bardwell, J. C. (2000) Redox switch of hsp33 has a novel zinc-binding motif. *J Biol Chem* **275**, 38302-38310
43. Lee, C., Lee, S. M., Mukhopadhyay, P., Kim, S. J., Lee, S. C., Ahn, W. S., Yu, M. H., Storz, G., and Ryu, S. E. (2004) Redox regulation of OxyR requires specific disulfide bond formation involving a rapid kinetic reaction path. *Nat Struct Mol Biol* **11**, 1179-1185
44. Antelmann, H., and Helmann, J. D. (2011) Thiol-based redox switches and gene regulation. *Antioxidants & redox signaling* **14**, 1049-1063
45. Finn, R. D., Bateman, A., Clements, J., Coggill, P., Eberhardt, R. Y., Eddy, S. R., Heger, A., Hetherington, K., Holm, L., Mistry, J., Sonnhammer, E. L., Tate, J., and Punta, M. (2014) Pfam: the protein families database. *Nucleic Acids Res* **42**, D222-230
46. Baba, T., Ara, T., Hasegawa, M., Takai, Y., Okumura, Y., Baba, M., Datsenko, K. A., Tomita, M., Wanner, B. L., and Mori, H. (2006) Construction of Escherichia coli K-12 in-frame, single-gene knockout mutants: the Keio collection. *Mol Syst Biol* **2**, 2006 0008

bioRxiv preprint doi: https://doi.org/10.1101/613315; this version posted April 1, 2020. The copyright holder for this preprint (which was not certified by peer review) is the author/funder, who has granted bioRxiv a license to display the preprint in perpetuity. It is made available under aCC-BY-NC 4.0 International license.

47. Nichols, R. J., Sen, S., Choo, Y. J., Beltrao, P., Zietek, M., Chaba, R., Lee, S., Kazmierczak, K. M., Lee, K. J., Wong, A., Shales, M., Lovett, S., Winkler, M. E., Krogan, N. J., Typas, A., and Gross, C. A. (2011) Phenotypic landscape of a bacterial cell. *Cell* **144**, 143-156
48. Itoh, T., Aiba, H., Baba, T., Hayashi, K., Inada, T., Isono, K., Kasai, H., Kimura, S., Kitakawa, M., Kitagawa, M., Makino, K., Miki, T., Mizobuchi, K., Mori, H., Mori, T., Motomura, K., Nakade, S., Nakamura, Y., Nashimoto, H., Nishio, Y., Oshima, T., Saito, N., Sampei, G., Seki, Y., Horiuchi, T., and et al. (1996) A 460-kb DNA sequence of the Escherichia coli K-12 genome corresponding to the 40.1-50.0 min region on the linkage map. *DNA Res* **3**, 379-392
49. Oliver, D. B. (1985) Identification of five new essential genes involved in the synthesis of a secreted protein in Escherichia coli. *J Bacteriol* **161**, 285-291
50. Sandikci, A., Gloge, F., Martinez, M., Mayer, M. P., Wade, R., Bukau, B., and Kramer, G. (2013) Dynamic enzyme docking to the ribosome coordinates N-terminal processing with polypeptide folding. *Nat Struct Mol Biol* **20**, 843-850
51. Miller, J. H. (1992) *A Short Course in Bacterial Genetics*, Cold Spring Harbor Press, Cold Spring Harbor, NY
52. Grabowicz, M., Yeh, J., and Silhavy, T. J. (2013) Dominant negative lptE mutation that supports a role for LptE as a plug in the LptD barrel. *J Bacteriol* **195**, 1327-1334
53. Huber, D., Rajagopalan, N., Preissler, S., Rocco, M. A., Merz, F., Kramer, G., and Bukau, B. (2011) SecA interacts with ribosomes in order to facilitate posttranslational translocation in bacteria. *Mol Cell* **41**, 343-353
54. Andreasson, C., Fiaux, J., Rampelt, H., Mayer, M. P., and Bukau, B. (2008) Hsp110 is a nucleotide-activated exchange factor for Hsp70. *J Biol Chem* **283**, 8877-8884
55. Clubb, R. T., Thanabal, V., and Wagner, G. (1992) A Constant-Time 3-Dimensional Triple-Resonance Pulse Scheme to Correlate Intraresidue H-1(N), N-15, and C-13(') Chemical-Shifts in N-15-C-13-Labeled Proteins. *Journal of magnetic resonance* **97**, 213-217
56. Grzesiek, S., and Bax, A. (1992) Improved 3d Triple-Resonance Nmr Techniques Applied to a 31-Kda Protein. *Journal of magnetic resonance* **96**, 432-440
57. Lescop, E., Schanda, P., and Brutscher, B. (2007) A set of BEST triple-resonance experiments for time-optimized protein resonance assignment. *Journal of magnetic resonance* **187**, 163-169
58. Kay, L. E., Keifer, P., and Saarinen, T. (1992) Pure Absorption Gradient Enhanced Heteronuclear Single Quantum Correlation Spectroscopy with Improved Sensitivity. *Journal of the American Chemical Society* **114**, 10663-10665
59. Salzmann, M., Wider, G., Pervushin, K., Senn, H., and Wuthrich, K. (1999) TROSY-type triple-resonance experiments for sequential NMR assignments of large proteins. *Journal of the American Chemical Society* **121**, 844-848
60. Schanda, P., Van Melckebeke, H., and Brutscher, B. (2006) Speeding up three-dimensional protein NMR experiments to a few minutes. *Journal of the American Chemical Society* **128**, 9042-9043
61. Salzmann, M., Pervushin, K., Wider, G., Senn, H., and Wuthrich, K. (1998) TROSY in triple-resonance experiments: New perspectives for sequential NMR assignment of large proteins. *P Natl Acad Sci USA* **95**, 13585-13590
62. Kazimierczuk, K., and Orekhov, V. Y. (2011) Accelerated NMR spectroscopy by using compressed sensing. *Angew Chem Int Ed Engl* **50**, 5556-5559
63. Delaglio, F., Grzesiek, S., Vuister, G. W., Zhu, G., Pfeifer, J., and Bax, A. (1995) NMRPipe: a multidimensional spectral processing system based on UNIX pipes. *J Biomol NMR* **6**, 277-293
64. Lee, W., Tonelli, M., and Markley, J. L. (2015) NMRFAM-SPARKY: enhanced software for biomolecular NMR spectroscopy. *Bioinformatics* **31**, 1325-1327
65. Case, D. A., Ben-Shalom, I. Y., Brozell, S. R., Cerutti, D. S., T.E. Cheatham, I., Cruzeiro, V. W. D., Darden, T. A., Duke, R. E., Ghoreishi, D., Gilson, M. K., Gohlke, H., Goetz, A. W., Greene, D., Harris, R., Homeyer, N., Izadi, S., Kovalenko, A., Kurtzman, T., Lee, T. S., LeGrand, S., Li, P., Lin, C., Liu, J., Luchko, T., Luo, R., Mermelstein, D. J., Merz, K. M., Miao, Y., Monard, G.,

bioRxiv preprint doi: https://doi.org/10.1101/613315; this version posted April 1, 2020. The copyright holder for this preprint (which was not certified by peer review) is the author/funder, who has granted bioRxiv a license to display the preprint in perpetuity. It is made available under aCC-BY-NC 4.0 International license.

Nguyen, C., Nguyen, H., Omelyan, I., Onufriev, A., Pan, F., Qi, R., Roe, D. R., Roitberg, A., Sagui, C., Schott-Verdugo, S., Shen, J., Simmerling, C. L., Smith, J., Salomon-Ferrer, R., Swails, J., Walker, R. C., Wang, J., Wei, H., Wolf, R. M., Wu, X., Xiao, L., York, D. M., and Kollman, P. A. (2018) AMBER 2018. University of California, San Francisco

66. Maier, J. A., Martinez, C., Kasavajhala, K., Wickstrom, L., Hauser, K. E., and Simmerling, C. (2015) ff14SB: Improving the Accuracy of Protein Side Chain and Backbone Parameters from ff99SB. *J Chem Theory Comput* **11**, 3696-3713
67. Pang, Y. P. (1999) Novel zinc protein molecular dynamics simulations: Steps toward antiangiogenesis for cancer treatment. *J Mol Model* **5**, 196-202
68. Li, P. F., Roberts, B. P., Chakravorty, D. K., and Merz, K. M. (2013) Rational Design of Particle Mesh Ewald Compatible Lennard-Jones Parameters for +2 Metal Cations in Explicit Solvent. *J Chem Theory Comput* **9**, 2733-2748
69. Li, P. F., and Merz, K. M. (2014) Taking into Account the Ion-Induced Dipole Interaction in the Nonbonded Model of Ions. *J Chem Theory Comput* **10**, 289-297
70. Li, P. F., Song, L. F., and Merz, K. M. (2015) Systematic Parameterization of Monovalent Ions Employing the Nonbonded Model. *J Chem Theory Comput* **11**, 1645-1657
71. Li, P. F., Song, L. F., and Merz, K. M. (2015) Parameterization of Highly Charged Metal Ions Using the 12-6-4 LJ-Type Nonbonded Model in Explicit Water. *J Phys Chem B* **119**, 883-895
72. Pettersen, E. F., Goddard, T. D., Huang, C. C., Couch, G. S., Greenblatt, D. M., Meng, E. C., and Ferrin, T. E. (2004) UCSF Chimera--a visualization system for exploratory research and analysis. *J Comput Chem* **25**, 1605-1612

FIGURE LEGENDS

Figure 1. Effect of azide on the C-terminal tail of SecA. (A) Plot of the degree of depletion or enrichment in transposon insertions in all of the non-essential genes in *E. coli* after growth of the TraDIS library to OD_{600} = 0.9 in the presence of 0.5 mM sodium azide. The $\log_2$ of the fraction of the number of insertions in a gene after growth in the presence of 0.5 mM azide over the number of insertions after growth in LB was plotted according to the degree of enrichment. Data points representing insertions in the *secA*, *secF*, *secG*, *secM*, *yidC*, *yajC*, *cpxR*, *dsbA*, *ahpC*, *gor* and *trxC* genes are indicated. Single gene deletion mutants that were compared to growth of the parent in **table 1** are indicated (bold). (B) Number of mutants containing insertions at the indicated location in the *secA* gene after growth of the TraDIS library in the absence (black) or presence of 0.25 (blue) or 0.5 mM (red) NaN_3. Most of these insertions truncate the *secA* gene between codons 822 and 829 at the junction between the HSD and the CTT. (C) Cultures of *E. coli* producing His-SUMO-SecA (lanes 1-4) or His-SUMO-SecA$^{CC/AA}$ (lanes 5& 6) were grown to late exponential phase. In the case of His-SUMO-SecA, half of the culture was treated with 2 mM sodium azide for 10 minutes prior to lysis (lanes 3 & 4), and the other half was left untreated (lanes 1 & 2). His-SUMO-SecA and SUMO-SecA$^{CC/AA}$ were purified from the cell lysates using Ni-affinity purification. Phospholipids from 2 mg of the purified protein were extracted into 100 µl chloroform, and 5µl of the extracted phospholipids (lanes 1, 3 and 6) and the wash buffer (lanes 2, 4 and 5) were resolved using thin-layer chromatography (TLC). The positions of phosphatidylglycerol (PG), phosphatidylethanolamine (PE) and cardiolipin (CL) are indicated.

Figure 2. The SecA MBD copurifies with iron and binds to iron *in vitro*. (A) Cells producing SUMO-CTT were incubated in the absence (untreated) or presence (+N_3) of 2 mM NaN_3 for 10 minutes. SUMO-CTT was purified from the cell lysates using streptactin beads and washed extensively with buffer. The iron content of SUMO-CTT was determined using mass spectrometry (ICP-MS) and normalised to the protein concentration in the eluted protein. Confidence intervals are one s.d. (B) DRH839 cells (Δ*secA* p_{trc}-*secA-biotin*) were grown in the presence of 10 µM or 1 mM IPTG to induce expression of SecA-biotin. Cells were rapidly lysed by cell disruption, incubated with streptavidin-sepharose and washed extensively with

bioRxiv preprint doi: https://doi.org/10.1101/613315; this version posted April 1, 2020. The copyright holder for this preprint (which was not certified by peer review) is the author/funder, who has granted bioRxiv a license to display the preprint in perpetuity. It is made available under aCC-BY-NC 4.0 International license.

buffer. The zinc and iron content of the EDTA eluate was determined using ICP-OES and normalised to the amount of protein bound to the streptavidin beads. An estimation of the concentrations of SecA and streptavidin in the purified protein suggested that SecA copurified with stoichiometric amounts of iron. (C) The echo-detected field swept EPR spectrum of oxidised $FeSO_4$ was determined in the absence (blue trace) or presence (red trace) of SecA-MBD.

Figure 3. Spectroscopic analysis of metal binding by YecA and YchJ. (A) His-SUMO-YecA and His-SUMO-YchJ were purified using Ni-affinity chromatography, and the amount of co-purifying Zn, Mn, Co, Cu and Fe were determined by ICP-MS. The concentrations of the extracted metals were normalised to the amount of purified protein. Confidence intervals are one standard deviation. (B) Buffer subtracted absorbance spectra of purified YecA (solid black), purified YecA that was dialysed against EDTA (dash-dot) and EDTA-dialysed YecA to which an equimolar concentration of $FeSO_4$ was added (dashed). The absorbance spectra were normalised to the concentration of YecA. (C) The echo-detected field swept EPR spectrum of $FeCl_3$ was determined in the absence (blue trace) or presence (red trace) of YecA.

Figure 4. YecA binds to iron *via* its MBD. (A) TROSY spectrum of metal-free ^{15}N & ^{13}C-labelled YecA. The ^{1}H, ^{15}N, and ^{13}C resonances of the polypeptide backbone for the C-terminal 20 amino acids (excluding prolines-206 and -208) were assigned using triple resonance experiments. Resonances of amino acids in the MBD are indicated with arrowheads. Amino acids producing two resonance peaks are labelled in green. (B) Overlay of the TROSY spectra of metal-free YecA (red) and YecA in the presence of equimolar concentrations of $FeSO_4$ (blue). The absence of a blue peak suggests that the amino acid producing the resonance is in the proximity of the bound iron.

Figure 5. ^{1}H-NMR analysis of metal binding by SecA-MBD and SecA-MBD^{S889A}. (A) 6.5-10 ppm region of the ^{1}H-NMR spectra of SecA-MBD in the absence (blue) or presence of equimolar concentrations of $FeSO_4$ (red) or $ZnSO_4$ (green). The appearance of resonances in the ~8.5-10 ppm region in the presence of $ZnSO_4$ indicates the formation of secondary structure. The strong quenching of the resonances in the presence of $FeSO_4$ is due to proximity to the bound iron ion. (B) 0.2-1.0 ppm region of the ^{1}H-NMR spectra of SecA-MBD in the absence (blue) or presence of equimolar concentrations of $FeSO_4$ (red) or $ZnSO_4$ (green). Binding of SecA-MBD to zinc results in a shift of the resonances corresponding to the methyl ^{1}Hs of valine, and binding of SecA-MBD to iron results in a significant broadening and flattening of these resonances. (C & D) 0.2-1.0 ppm region of the ^{1}H-NMR spectra of SecA-MBD (C) or SecA-MBD^{S889A} (D) in the absence of metal (blue), in the presence of equimolar $FeSO_4$ (red) and after the addition of competing concentrations of $ZnSO_4$ to the iron-bound peptide after >10 minutes of equilibration at room temperature (purple).

Figure 6. Structural models of octahedral metal coordination. Ribbon diagrams of example structural models of the MBD coordinating a hexavalent metal using the δ-nitrogen (A) and the ε-nitrogen (B) of His-897 generated using molecular dynamic simulations. Example structures from each 1 ns of the final 10 ns of each 100 ns simulation can be found in the online supporting data. The side chains of the metal-coordinating amino acids are depicted as sticks (yellow, sulfur; blue, nitrogen; red, oxygen). Images were rendered using UCSF Chimera v. 1.12 (72).

bioRxiv preprint doi: https://doi.org/10.1101/613315; this version posted April 1, 2020. The copyright holder for this preprint (which was not certified by peer review) is the author/funder, who has granted bioRxiv a license to display the preprint in perpetuity. It is made available under aCC-BY-NC 4.0 International license.

Table 1. Relative growth rates of single gene deletion mutants in the absence and presence of sodium azide.

Strain	Growth rates*		
	LB	**0.25 mM NaN_3**	**0.5 mM NaN_3**
BW25113	1.00 ± 0.00	1.00 ± 0.09	1.00 ± 0.09
Δ*yajC*	0.88 ± 0.05	0.59 ± 0.08	0.54 ± 0.11
Δ*secG*	1.02 ± 0.05	0.53 ± 0.11	0.75 ± 0.1
Δ*dsbA*	1.01 ± 0.08	0.95 ± 0.09	0.63 ± 0.15
Δ*cpxR*	1.13 ± 0.13	0.93 ± 0.02	0.65 ± 0.15
Δ*gor*	0.96 ± 0.01	0.97 ± 0.08	1.02 ± 0.04
Δ*ahpC*	0.95 ± 0.00	0.80 ± 0.06	0.64 ± 0.06
Δ*trxC*	0.92 ± 0.00	0.89 ± 0.02	0.78 ± 0.04
MC4100	1.00 ± 0.02	ND†	1.00 ± 0.03
secA827::IS*1*	1.03 ± 0.01	ND†	1.38 ± 0.18

*Parent and mutants were grown in LB or LB containing the indicated concentration of sodium azide. Growth rates were determined by measuring the optical density at 600 nm every 30 minutes and normalised to the rate of growth of the parent strain under the same conditions.

†not determined

bioRxiv preprint doi: https://doi.org/10.1101/613315; this version posted April 1, 2020. The copyright holder for this preprint (which was not certified by peer review) is the author/funder, who has granted bioRxiv a license to display the preprint in perpetuity. It is made available under aCC-BY-NC 4.0 International license.

FIGURE 1.

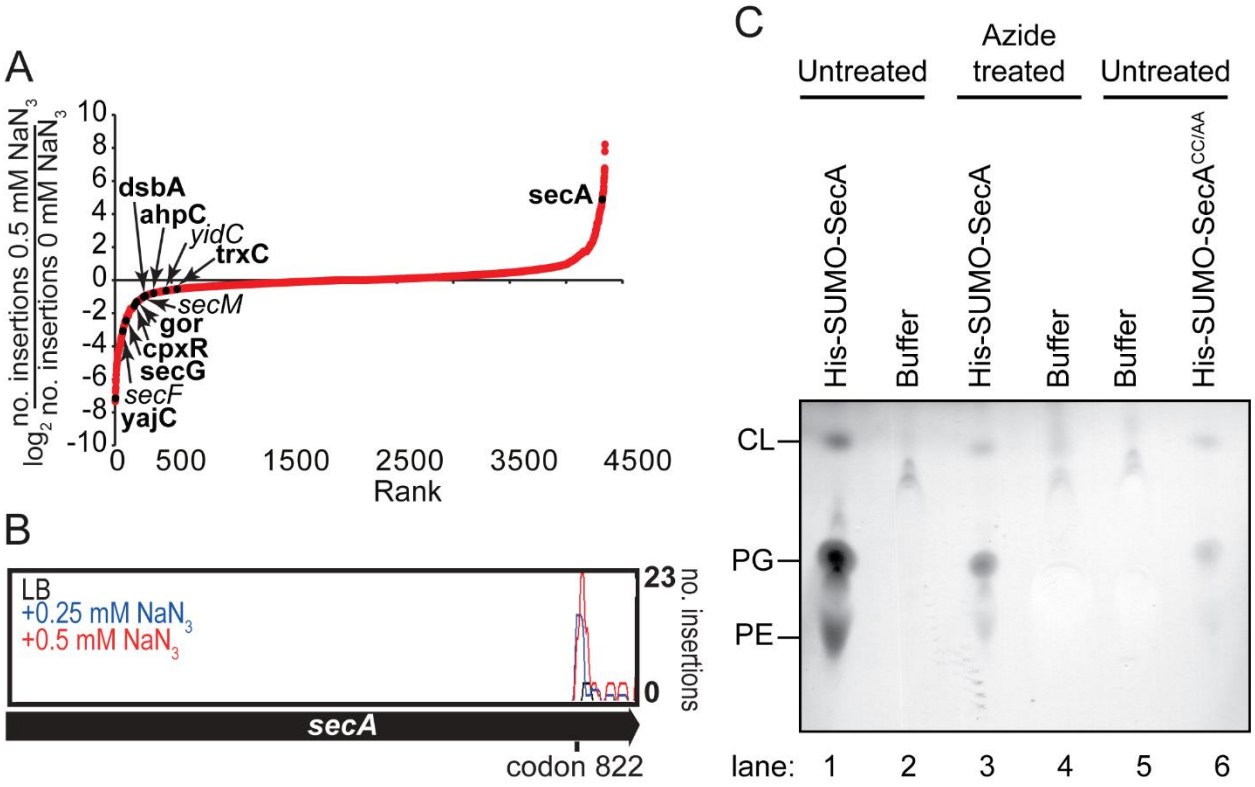

bioRxiv preprint doi: https://doi.org/10.1101/613315; this version posted April 1, 2020. The copyright holder for this preprint (which was not certified by peer review) is the author/funder, who has granted bioRxiv a license to display the preprint in perpetuity. It is made available under aCC-BY-NC 4.0 International license.

FIGURE 2.

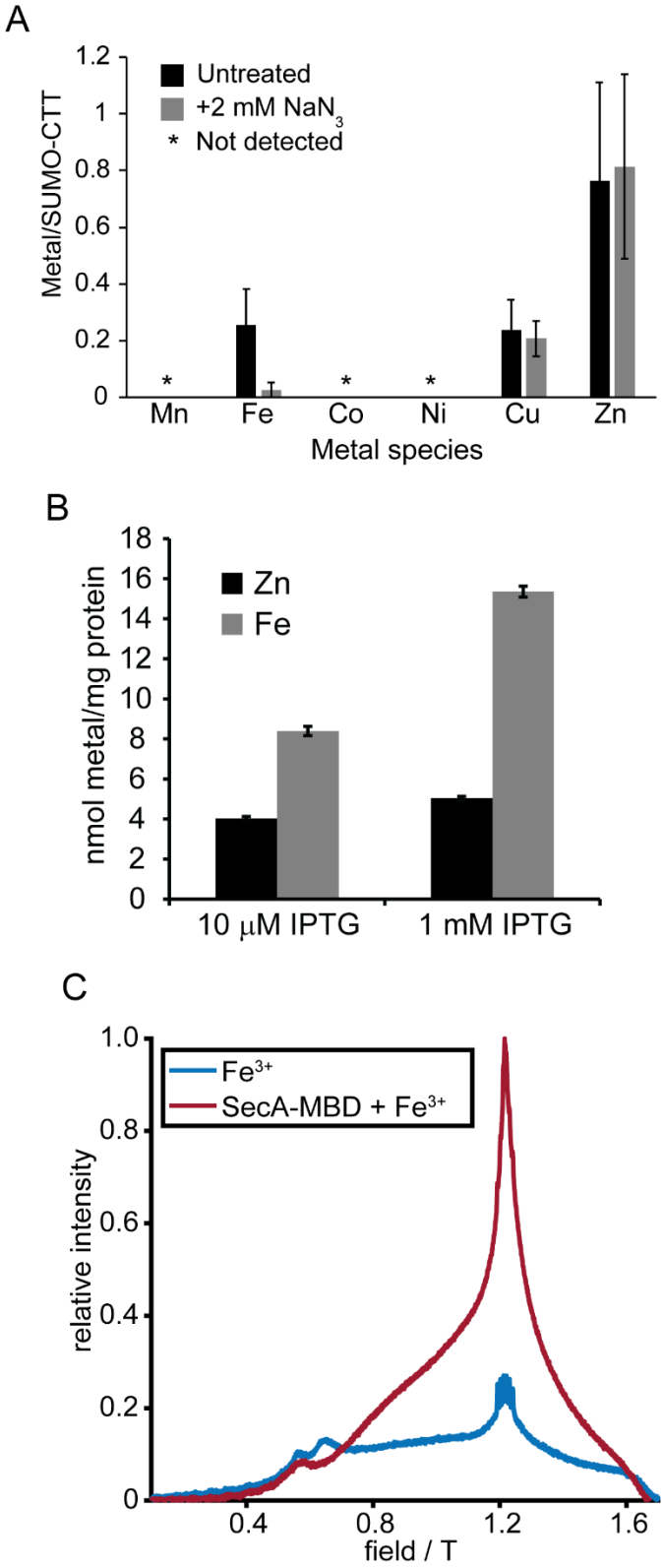

bioRxiv preprint doi: https://doi.org/10.1101/613315; this version posted April 1, 2020. The copyright holder for this preprint (which was not certified by peer review) is the author/funder, who has granted bioRxiv a license to display the preprint in perpetuity. It is made available under aCC-BY-NC 4.0 International license.

FIGURE 3.

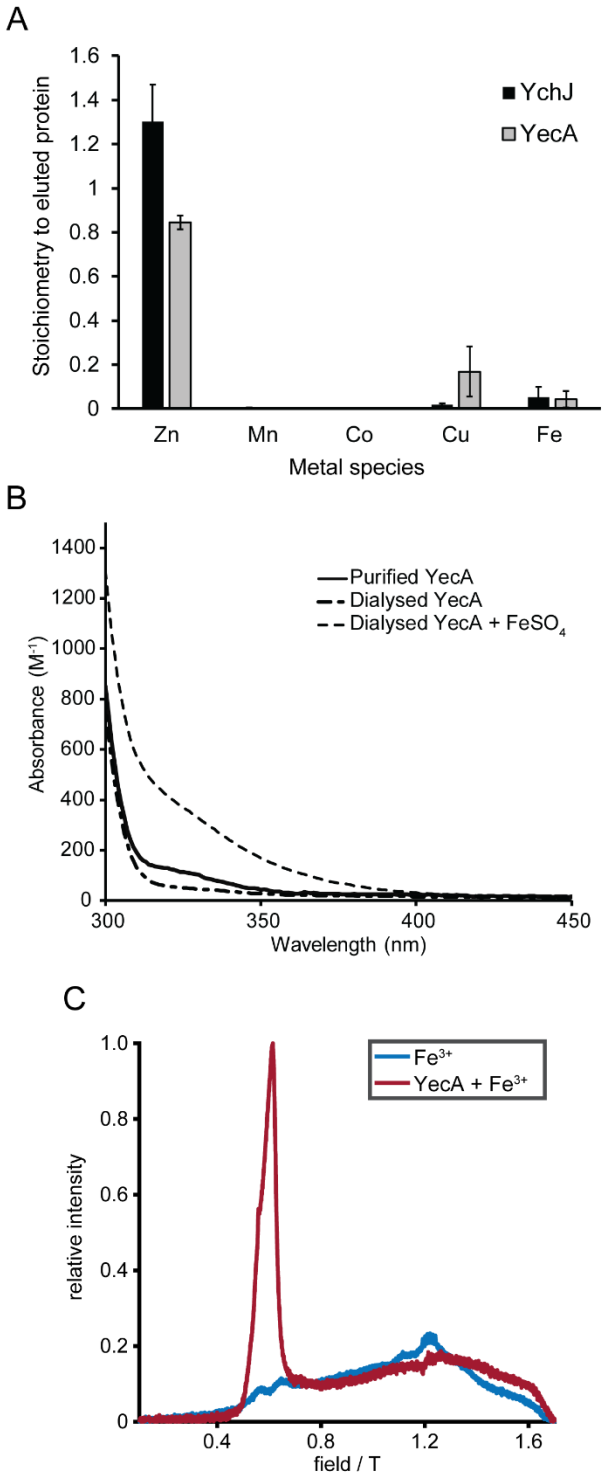

bioRxiv preprint doi: https://doi.org/10.1101/613315; this version posted April 1, 2020. The copyright holder for this preprint (which was not certified by peer review) is the author/funder, who has granted bioRxiv a license to display the preprint in perpetuity. It is made available under aCC-BY-NC 4.0 International license.

FIGURE 4.

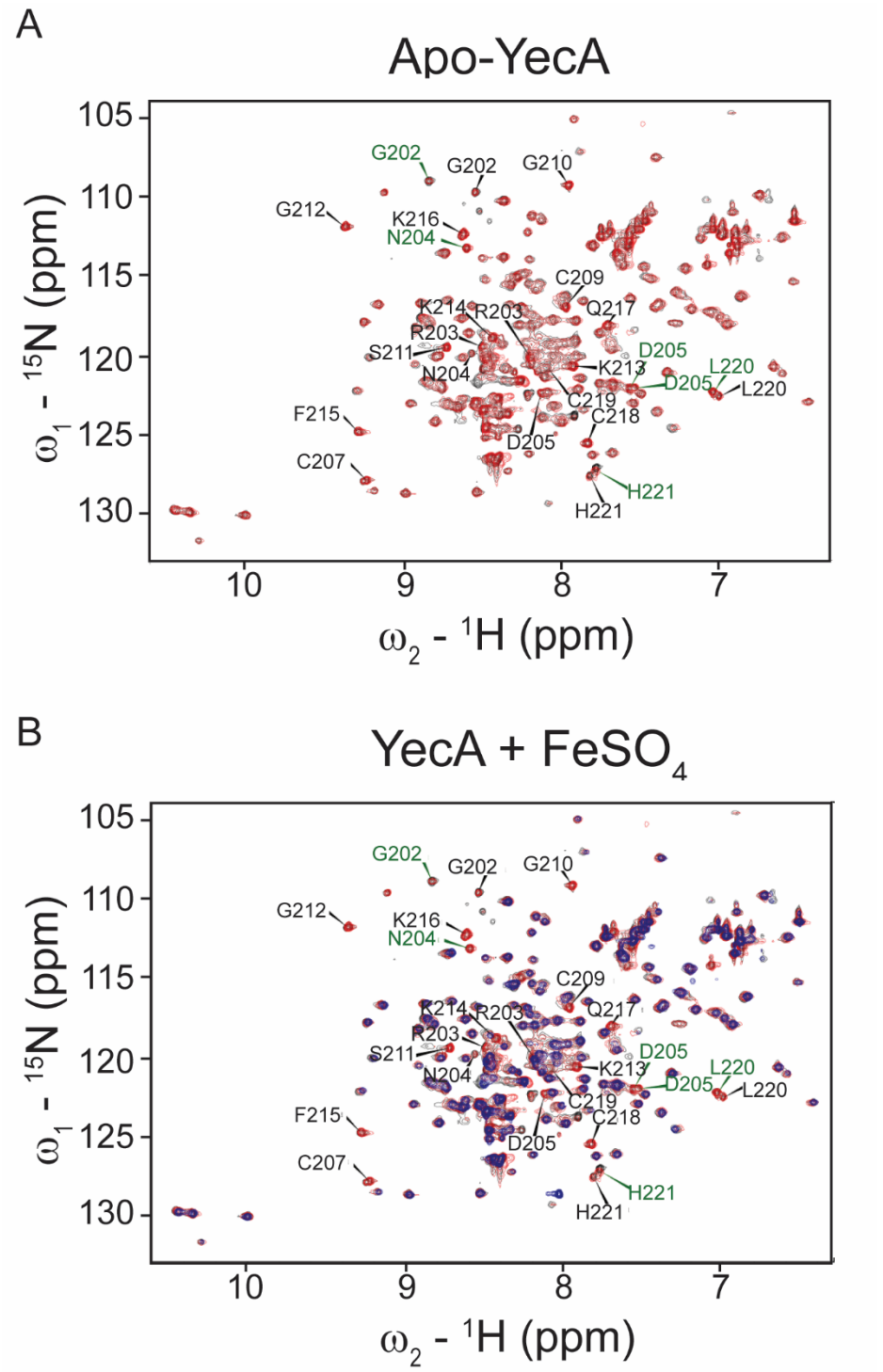

bioRxiv preprint doi: https://doi.org/10.1101/613315; this version posted April 1, 2020. The copyright holder for this preprint (which was not certified by peer review) is the author/funder, who has granted bioRxiv a license to display the preprint in perpetuity. It is made available under aCC-BY-NC 4.0 International license.

FIGURE 5.

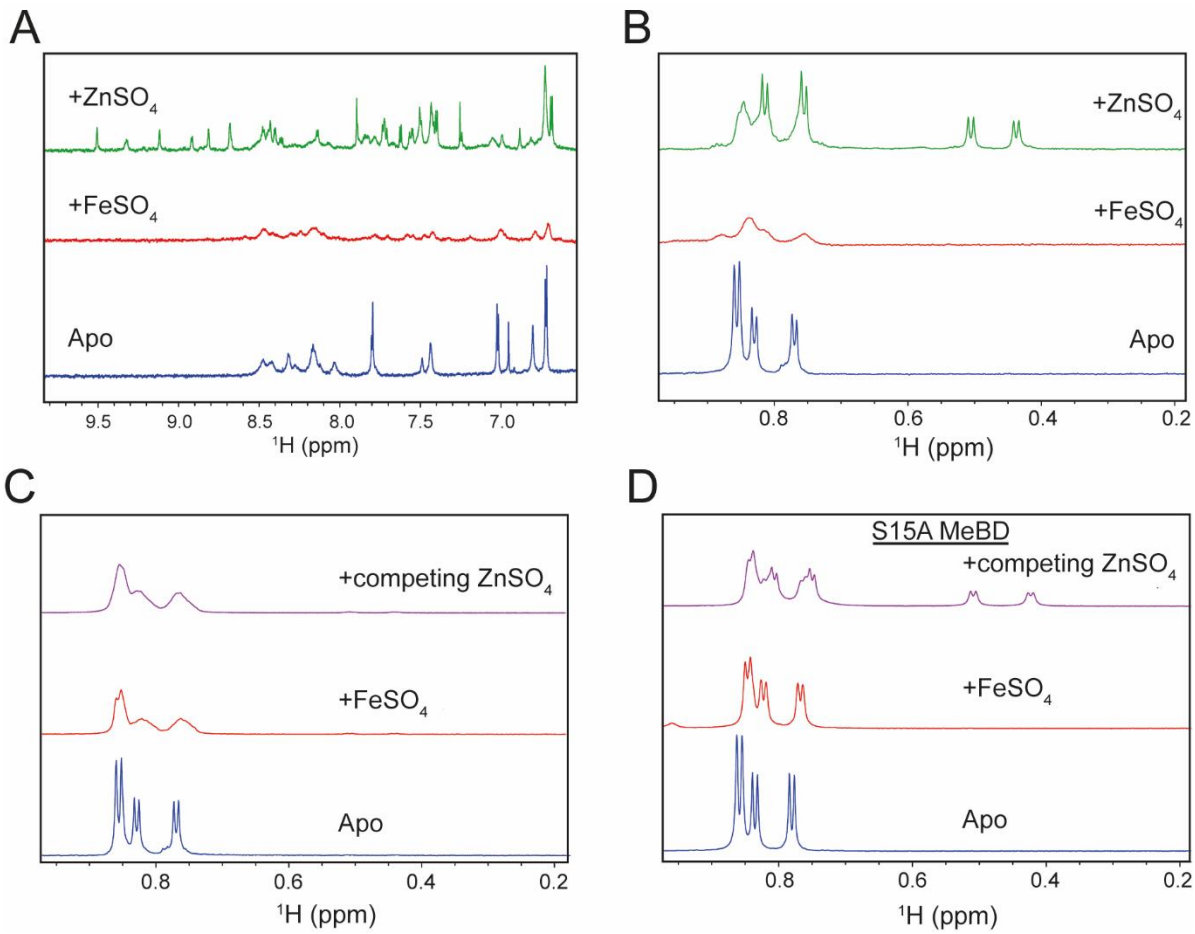

bioRxiv preprint doi: https://doi.org/10.1101/613315; this version posted April 1, 2020. The copyright holder for this preprint (which was not certified by peer review) is the author/funder, who has granted bioRxiv a license to display the preprint in perpetuity. It is made available under aCC-BY-NC 4.0 International license.
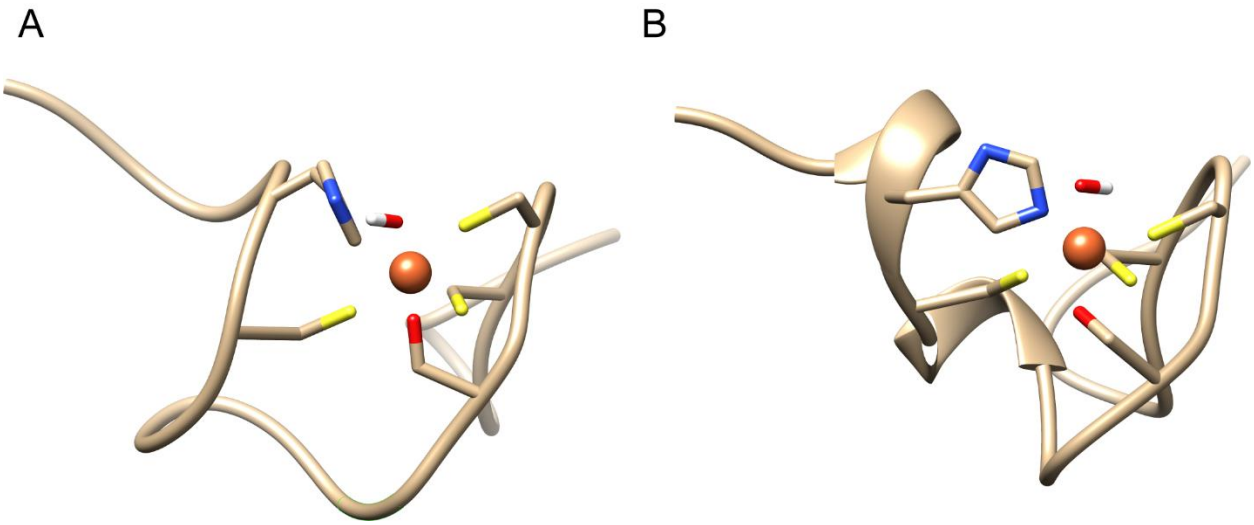
FIGURE 6.